NeuroImage 209 (2020) 116516

Contents lists available at ScienceDirect

NeuroImage

journal homepage: www.elsevier.com/locate/neuroimage

In vivo functional localization of the temporal monocular crescent representation in human primary visual cortex

Shahin Nasr [a,b,*], Cristen LaPierre [a], Christopher E. Vaughn [a], Thomas Witzel [a,b], Jason P. Stockmann [a,b], Jonathan R. Polimeni [a,b,c]

[a] Athinoula A. Martinos Center for Biomedical Imaging, Massachusetts General Hospital, Charlestown, MA, 02129, United States
[b] Harvard Medical School, Boston, MA, United States
[c] Massachusetts Institute of Technology, Division of Health Sciences and Technology, Cambridge, MA, United States

ARTICLE INFO

Keywords:
TMC
Blind spot
Functional MRI
MRI-Compatible goggles
V1
Visuotopy

ABSTRACT

The temporal monocular crescent (TMC) is the most peripheral portion of the visual field whose perception relies solely on input from the ipsilateral eye. According to a handful of post-mortem histological studies in humans and non-human primates, the TMC is represented visuotopically within the most anterior portion of the primary visual cortical area (V1). However, functional evidence of the TMC visuotopic representation in human visual cortex is rare, mostly due to the small size of the TMC representation (~6% of V1) and due to the technical challenges of stimulating the most peripheral portion of the visual field inside the MRI scanner. In this study, by taking advantage of custom-built MRI-compatible visual stimulation goggles with curved displays, we successfully stimulated the TMC region of the visual field in eight human subjects, half of them right-eye dominant, inside a 3 T MRI scanner. This enabled us to localize the representation of TMC, along with the blind spot representation (another visuotopic landmark in V1), in all volunteers, which match the expected spatial pattern based on prior anatomical studies. In all hemispheres, the TMC visuotopic representation was localized along the peripheral border of V1, within the most anterior portion of the calcarine sulcus, without any apparent extension into the second visual area (V2). We further demonstrate the reliability of this localization within/across experimental sessions, and consistency in the spatial location of TMC across individuals after accounting for inter-subject structural differences.

1. Introduction

In humans, the visual field subtends approximately 200° of visual angle laterally along the horizontal meridian (±100° horizontal eccentricity). However, functional MRI (fMRI) studies typically focus on neural mechanisms underlying responses to stimuli presented within the central (<10°) of the visual field. This is in part due to greater interest in central vision, perhaps due to the higher spatial encoding precision in central compared to peripheral vision, but also because of technical challenges faced with delivering stimuli to the visual field periphery during the fMRI experiment, which are especially difficult to overcome when using modern, conventional receive coil arrays. For these reasons, neural mechanisms underlying stimulus encoding within more peripheral visual fields have remained understudied (Pitzalis et al., 2006; Stenbacka and Vanni, 2007; Wu et al., 2012).

Stimulus encoding in the peripheral visual fields is coarser compared to the central visual field (Wilson, 1990; Duncan and Boynton, 2003). This is mainly due to the larger receptive fields of neurons within the cortical representation of these regions compared to those representing the central visual field (Daniel and Whitteridge, 1961; Gattass et al., 1987; Smith et al., 2001; Dumoulin and Wandell, 2008). However, information received from peripheral visual fields improves visual object processing (Pollatsek et al., 1990; Henderson and Anes, 1994), influences the direction of eye movement during visual search (Rosenholtz et al., 2012) and is crucial in navigation (Barton et al., 2014). The peripheral visual field (defined as >10° eccentricity) can be divided into two regions based on whether it can be seen by one or both eyes. One region extends to approximately 60° of the visual field and is seen *binocularly*, with exception of the blind spot (Young, 1801). The other region, known as the temporal monocular crescent (TMC), extends from approximately 60°–100° eccentricity to the temporal border of the far-peripheral visual field and is seen *monocularly* only by the ipsilateral eye.

* Corresponding author. Athinoula A. Martinos Center for Biomedical Imaging, 149 13th Street, Charlestown, MA, 02129, United States.
E-mail address: shahin@nmr.mgh.harvard.edu (S. Nasr).

https://doi.org/10.1016/j.neuroimage.2020.116516
Received 22 October 2019; Received in revised form 2 December 2019; Accepted 1 January 2020
Available online 3 January 2020
1053-8119/© 2020 The Author(s). Published by Elsevier Inc. This is an open access article under the CC BY-NC-ND license (http://creativecommons.org/licenses/by-nc-nd/4.0/).

Although the TMC representation within the cortical topographic map of the visual field (i.e., the visuotopic map) has been localized histologically in human primary visual cortex (V1) (Adams et al., 2007), to our knowledge, *in vivo* functional evidence of the visuotopic representation of this region within the human visual cortex is limited to one early study by Toosy et al. in which authors reported greater contralateral fMRI responses to monocular visual stimulation within the "presumed striate cortex" (Toosy et al., 2001). However, the exact location and spatial pattern of this activity relative to the borders of primary visual cortex, its potential extension into the adjacent secondary visual area, and consistency of the exact location of this small region across individuals remains unknown.

This lack of knowledge about the TMC representation within the human visual cortex is mainly due to: (*i*) technical difficulties in stimulation of this far peripheral region of the visual field using the conventional methods of stimulus presentation in the bore of an MRI scanner (Greco et al., 2016), (*ii*) the requirement to measure the 2D layout of the TMC representation along the cortex, within individual subjects, and (*iii*) the requirement of relatively high spatial resolution in order to verify that the geometry of the TMC representation matches with the spatial pattern known from prior anatomical studies. Specifically, according to histological studies in humans (Horton et al., 1990; Adams et al., 2007) and non-human primates (Horton and Hocking, 1996), the TMC is represented visuotopically by neurons within the most anterior portion of V1. Consistent with the well-known cortical magnification factor (Daniel and Whitteridge, 1961; Van Essen et al., 1984; Engel et al., 1997; Slotnick et al., 2001; Polimeni et al., 2006; Wandell et al., 2007), it has been shown that this large portion of the visual field is represented in humans by only ~6% of the total area of V1 (i.e., on average ~160 mm^2) (Horton et al., 1990; Adams et al., 2007). Mapping such a small brain region reliably relative to the borders of striate visual cortex requires a high-resolution neuroimaging technique with sufficient sensitivity to detect this representation in individual subjects (i.e., without requiring group averaging) in combination with accurate striate cortex localization.

To overcome these technical difficulties, in this study, we have used custom-built MRI-compatible goggles capable of independently stimulating each eye to localize the visuotopic representation of the TMC in humans *in vivo*. The curved displays within these goggles have enabled us to stimulate the entire visual field during the fMRI acquisition. In combination with high-resolution neuroimaging techniques and precise mapping of striate cortex borders (Hinds et al., 2008), this method of visual stimulation enabled us to localize the TMC representation in all tested individuals ($n = 8$) within the most anterior portion of V1. Besides the TMC, we have also localized the visuotopic representation of the blind spot (i.e., the gap in the perceived visual field caused by the optic disc of the retina), which is smaller in area compared to the TMC representation (Horton et al., 1990; Adams et al., 2007) and is expected to be approximately 17.5 mm^2 based on extrapolating the measurements of its size from measurement in macaque monkeys (Horton and Hocking, 1996) assuming a 175% scaling of the area of V1 between macaques and humans (Tootell and Taylor, 1995). The blind spot representation similarly receives purely monocular input and is located outside of the region of the visual field stimulated using conventional stimuli (Tootell et al., 1998; Awater et al., 2005).

2. Methods

2.1. Participants

Eight human volunteers (4 female), aged 24–41 years old, participated in this study. Among them, four subjects (two female) were right-eye dominant and the others were left-eye dominant, as assessed by hole-in-card test (i.e., the Dolman method) (Rice et al., 2008; Li et al., 2010). All subjects had normal or corrected-to-normal vision and no history of neurological or psychiatric illness. All procedures were in compliance with the guidelines of the Institutional Review Board of the Massachusetts General Hospital. Procedures were fully explained to all subjects, and informed written consent was obtained before scanning in accordance with the Declaration of Helsinki.

2.2. Visual stimulus apparatus

To stimulate the entire visual field, including the far (>60°) periphery necessary to localize the representation of the TMC, we used custom-built MRI-compatible goggles (Fig. 1A). The goggles were approximately 190 mm wide in the left-right direction and 50 mm at their maximum extent in the head-foot direction. Non-magnetic, MRI-compatible white light-emitting diodes (LEDs) were mounted on two low-profile, flexible printed circuit boards, one for each eye, that were in turn fixed to a curved plastic frame (similar to what is used for conventional safety glasses). Foam padding was added to the frame to ensure subject comfort when the goggles were placed against the face and to block light coming from either the LEDs of the opposite eye or external light sources. The radial build of the goggles was minimized (<15 mm) to ensure that they would fit between the subject's face and the inside of the helmet-shaped RF receive coil array housing. A white translucent plastic layer was used to insulate the LEDs and to diffuse the light into a nearly uniform illumination pattern across the entire visual field. Circuit board designs and parts lists for building the goggles are available upon request.

Current was supplied to the LEDs using a power transistor connected to a 24-V power supply. A microcontroller (Arduino Uno Rev3, Arduino, Somerville, MA, USA) was used to gate the transistor to drive the LEDs using short pulses of current. The duty cycle and width of these pulses in turn determined the stimulus intensity. The microcontroller initiated the visual stimulus paradigm, specified as an operator-supplied text file, upon receiving a trigger pulse from the MRI scanner at the beginning of the fMRI time-series acquisition. To ensure safety inside the MRI scanner's transmit RF coil, inductive chokes were used both on the LED circuit board and at intervals of 20 cm along the cable used to supply power to the goggles (~$\lambda/10$ at the 3T Larmor frequency of 123.25 MHz). To test for potential heating of the goggle device caused by eddy currents or RF power absorption, the goggles were safety checked by running the scanner gradient coils and the RF transmit coil at a high duty cycle, and the goggles and cabling surface temperatures were measured before and after the test. In addition, to check for interactions with the scanner RF transmit coil, the pre-scan transmit adjust reference voltage was recorded for three configurations using a standard water phantom: (1) without the goggles present in the bore, (2) with the goggles added to the bore, then (3) with the goggle LEDs powered in the bore. The transmit adjust voltage differed by less than ±20% over the three conditions — which is similar to the expected scan-rescan precision of this adjustment measurement — and was assumed safe according to the safety test protocol.

After passing the safety tests, in one subject, to test for potential image artifacts caused by the goggles, we measured the impact of the goggles on the magnetic field or B_0 homogeneity by acquiring an axial set of B_0 field maps in the same three configurations listed above. Fig. 1B shows the magnitude images corresponding to the B_0 field map acquisitions, which depict the anatomical locations of the maps, and Fig. 1C–E shows, respectively, the B_0 field map itself measured in the subject (1) without wearing the goggles, (2) while wearing the goggles, then (3) while wearing the goggles during stimulation by the LEDs. As demonstrated, we did not find any apparent changes in the B_0 field map between these three configurations, indicating that the goggles did not introduce magnetic field inhomogeneity. Therefore we do not expect any geometric distortion of the fMRI data caused by the goggle materials, electronics, or electrical currents when the LEDs are powered.

2.3. Visual stimuli and paradigm

Using these goggles, we stimulated each eye separately (i.e., we used monocular stimulation only) by flashing the white-light LEDs (90 cd/m^2)

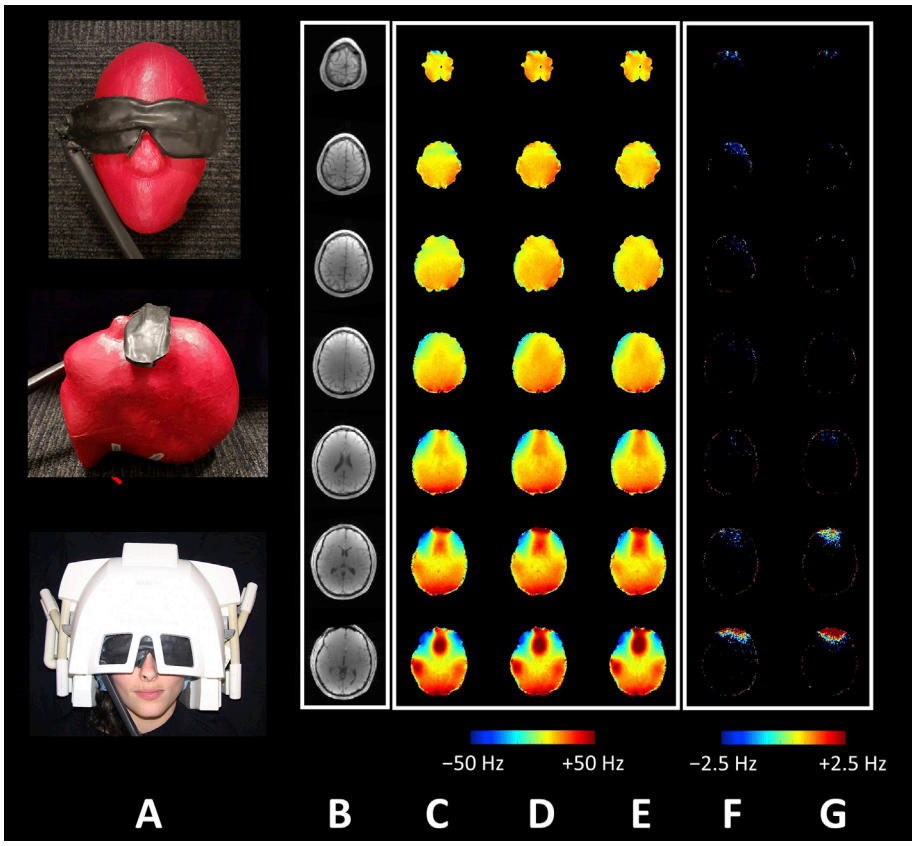

Fig. 1. The impact of the goggles on the magnetic field distribution assessed with conventional B_0 field maps acquired both with the goggles present but powered off and during LED flashing. Panel **A** consists of photographs of the goggles placed on a phantom (used for safety testing (see Methods)), shown from above and from the side, and on a volunteer within the RF head coil array housing. The goggle curved lenses enabled us to stimulate the whole visual field even within the MRI scanner. Panel **B** shows the anatomical locations of the B_0 field maps in 6 different axial slices (top-bottom: superior-inferior). To test whether the goggle apparatus could introduce B_0 inhomogeneity that would cause geometric distortion in our EPI data, we measured a conventional B_0 field map in one subject in three conditions: without the goggles, with the goggles positioned on the subject but without power, and with the goggles positioned on the subject with LED flashing similar to that used during our visual stimulation. The resulting B_0 field maps are presented in panels **C–E** respectively. Panels **F** and **G** directly show the difference in the B_0 fieldmap caused by goggle presence (without power and powered, respectively) relative to the B_0 fieldmaps acquired after the goggle apparatus was completely removed from the scanner. As demonstrated in these figures, we did not detect any apparent change in the B_0 field across these conditions, suggesting that our stimulus apparatus did not induce any geometric distortion in regions of interest (i.e., visual cortex in general and calcarine sulcus in particular).

flickering at a frequency of 8 Hz. The stimulated eye was alternated with a block-design paradigm (24 s per block). During the scans, subjects were asked to keep their eyes open throughout the stimulation and to blink normally.

In a separate experimental session, we mapped the cortical visuotopic representations of 1°, 4°, 7°, 10°, 13° and 16° visual field eccentricities using ring-shaped stimuli filled with conventional flashing (2 Hz) radially-scaled checkerboard patterns (Fig. 2A and B). The eccentricity mapping enabled us to confirm the visual field location of blind spot representation, which is expected to be around 12–15° (Adams et al., 2007). During this test, subjects were instructed to focus on a disc-shaped fixation target, presented at the left-most or right-most edge of the screen to allow for the stimulation of eccentricities out to 16°, and report its color change (from red to blue and vice versa) by pressing a key on an MR-compatible key pad. The location of the fixation target remained unchanged during a given run but changed randomly between runs, and subjects were informed about its whereabouts in advance prior to each scan.

In the same experimental session, we also mapped the cortical visuotopic representation of the horizontal and vertical meridians (Fig. 2C). During this test, subjects were instructed to carefully fixate a centrally-presented disc-shaped fixation target and to report its color change (from red to blue and vice versa) by pressing a key on a MR-compatible key pad. This test enabled us to define the borders of V1

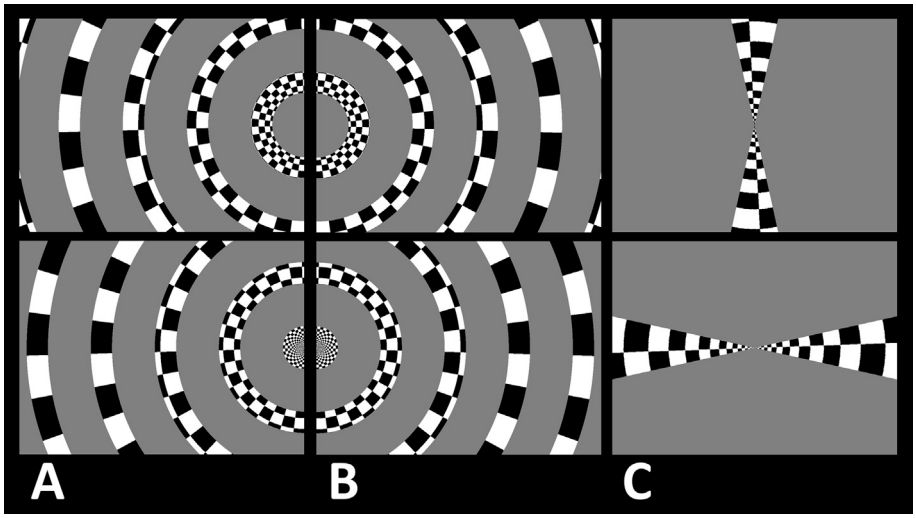

Fig. 2. Visual stimuli used for retinotopy mapping. Panels **A** and **B** show the stimuli used for stimulating visual cortex across 1°, 4°, 7°, 10°, 13°, 16°, 19°, 22°, 25° and 28° eccentricities within the left and right visual fields, respectively. Notably, the most peripheral ring could only be presented partially due to the limited size of screen. During the eccentricity mapping, subjects were asked to fixate a fixation target presented either on the right (Panel **A**) or the left (Panel **B**) side of screen to expand the stimulated region of their visual field laterally. Panel **C** shows the masked checkerboard stimuli used to define V1 borders functionally. By contrasting the response evoked by stimulation of horizontal vs. vertical meridians, while subjects fixated at a centrally presented fixation spot, borders of the primary visual area were defined within the central portion of V1 (eccentricity <10°). These borders were further compared (Fig. 3) relative to their localization based on structural landmarks (Hinds et al., 2008).

functionally, and to compare this functional localization relative to the prediction of the V1 boundaries based on structural landmarks derived from the cortical folding pattern reconstructed from each subject's anatomical data (Hinds et al., 2008).

2.4. Imaging

MRI data were collected with a 3T TimTrio whole-body human MRI scanner (Siemens Heathineers, Erlangen, Germany), with the standard vendor-supplied 32-channel head coil array. FMRI data were acquired using standard 2D gradient-echo BOLD-weighted EPI (TR = 3000 ms, TE = 32 ms, flip angle = 90°, in-plane acceleration factor $R = 3$, nominal echo spacing = 0.9 ms, no partial Fourier, voxel size = 1.2 × 1.2 × 1.2 mm^3, 41 slices, and FOV = 192 × 192 × 49.2 mm^3). The slices were positioned in an oblique-axial orientation centered on and parallel to the long axis of the calcarine sulcus, such that V1 and a portion of V2 was included in the fMRI acquisition. Each subject participated in 10 runs (12 blocks per run, 24 s per block, with each block starting and ending with a 12-s period of no stimulation). To test the reproducibility of our findings, the right-eye-dominant subjects ($n = 4$) participated in an extra session (on a separate day) during which we repeated the experiment with identical acquisition and stimulation parameters.

For all subjects we also collected anatomical reference data using a standard 3D T_1-weighted multi-echo MPRAGE pulse sequence with protocol parameter values: TR = 2530 ms, four echoes with $TE_1 = 1.64$ ms, $TE_2 = 3.5$ ms, $TE_3 = 5.36$ ms, $TE_4 = 7.22$ ms, TI = 1200 ms, flip angle = 7°, echo spacing = 10.3 ms, acceleration factor = 2, no partial Fourier, bandwidth = 651 Hz/pix, voxel size = 1.0 × 1.0 × 1.0 mm^3, FOV = 256 × 256 × 176 mm^3.

2.5. Data analysis

Functional and anatomical MRI data were pre-processed and analyzed using FreeSurfer and FS-FAST (version 6.0; http://surfer.nmr.mgh.harvard.edu) (Fischl, 2012). For each subject, cortical surfaces were reconstructed based on the T_1-weighted anatomical data after which both inflated and flattened representations were generated (Dale et al., 1999; Fischl et al., 1999, 2002). The complete border of V1, including the V1/V2 border, was defined anatomically using a surface-based atlas derived from microanatomical features (Hinds et al., 2008), and was generated automatically in FreeSurfer as part of the automatic cortical surface reconstruction and anatomical parcellation.

All functional images were rigidly aligned (6 DOF) to the subject's own anatomical reference scan using rigid Boundary-Based Registration (Greve and Fischl, 2009) and then corrected for motion. The motion-corrected functional data were then projected onto the cortical surface representation (corresponding to the mid-cortical depth) and spatially smoothed (2D Gaussian filtered with a 1.5 mm FWHM). A standard hemodynamic response model based on a gamma function was convolved with the stimulus timing to generate a task regressor for the fMRI signal which was used in a standard univariate General Linear Model framework to estimate the amplitude of the BOLD response in each voxel. For each individual subject, the average BOLD response maps were calculated for each condition (Friston et al., 1999). Finally, voxel-wise statistical tests were conducted and the resultant significance maps were projected into the subject's anatomical volumes and onto the corresponding reconstructed cortical surfaces.

Group-averaging was performed after resampling the activity maps onto a common surface-based brain template, *fsaverage* (Fischl, 2012). To test the consistency of the TMC representation location across individuals, group-averaged maps were generated using a random-effects model and corrected for multiple comparisons. A similar test was also applied to the blind spot representation to assess its localization consistency in the cortical hemisphere contralateral to the dominant eye for left- and right-eye-dominant subjects separately. Notably, activation within the blind spot representation in the ipsilateral hemisphere is expected to be weaker due to the lower response to stimulation of the non-dominant compared to dominant eye (Rombouts et al., 1996). However, due to the smaller number of subjects in the blind spot representation localization test compared to the TMC representation localization test mentioned above (i.e., $n = 4$ rather than $n = 8$), group-averaged activity maps were generated for the blind spot representation localization based on a fixed-effects model rather than a random-effects model (Fig. 5B). Due to the small size of the blind spot representation, correction for multiple comparisons was omitted.

2.6. Region of interest (ROI) analysis

To examine the activity within the TMC representation (i.e., our region of interest) across individual subjects, we used the results of group-averaged activity maps generated based on the random-effects analysis. In these activity maps we localized the TMC representations bilaterally, and defined the ROI based on the statistical map thresholded at $p < 10^{-2}$. The TMC representation ROIs were then transformed from the surface-based template (*fsaverage*) back into native space (i.e., each subject's own cortical surface reconstructed).

2.7. Data availability

Data are available on request from the authors.

3. Results

Histological studies in humans have shown that the visuotopic representation of the TMC is located within the most anterior portion of V1 and that in this region neurons respond only to stimulation of the contralateral eye (Adams et al., 2007). Here, we tested the activity evoked by left-vs. right-eye stimulation to test whether we could detect the TMC representation as a response preference for contralateral compared to ipsilateral eye stimulation in the anterior portion of V1. Fig. 3A and B shows the mapping of activity evoked by this contrast in one right-eye-dominant and one left-eye-dominant subject, respectively. As demonstrated in these data, we found a significantly ($p < 0.05$) stronger response to stimulation of contralateral compared to ipsilateral eye stimulation in the expected location of the TMC representation within the most anterior portion of V1. Interestingly this contralateral preference remained mostly within the borders of V1, as estimated structurally based on the cortical folding pattern (see Methods) (Hinds et al., 2008), with limited extension into neighboring V2 or the prostriata.

To further confirm our ability to detect monocular responses within V1, we tested whether we could localize the blind spot representation posterior to the TMC representation (Adams et al., 2007). Using more spatially-confined visual stimulation configurations, previous neuroimaging studies have successfully localized the blind spot representation in human subjects *in vivo* (Tootell et al., 1998; Tong and Engel, 2001; Awater et al., 2005). In these studies, the blind spot representation was localized close to the cortical representation of 15° eccentricity and roughly along (although slightly inferior to) the horizontal meridian representation. In agreement with these previous studies, we detected a region of monocular activation consistent with the location of the blind spot representation in all hemispheres contralateral to the dominant eye as an activity patch with higher response to ipsilateral compared to contralateral eye stimulation. This representation was located posteriorly relative to the TMC representation and near to albeit somewhat anterior to the cortical representation of 13° eccentricity (Fig. 3). In the ipsilateral hemispheres (relative to the dominant eye), we were only able to localize the blind spot representation in 50% of individuals (two of which were right-eye dominant), likely due to the lower or weaker evoked response to stimulation of the non-dominant eye (Rombouts et al., 1996).

We further tested the reliability of these V1 activity maps in two different ways. First, for all subjects, we measured the percent BOLD

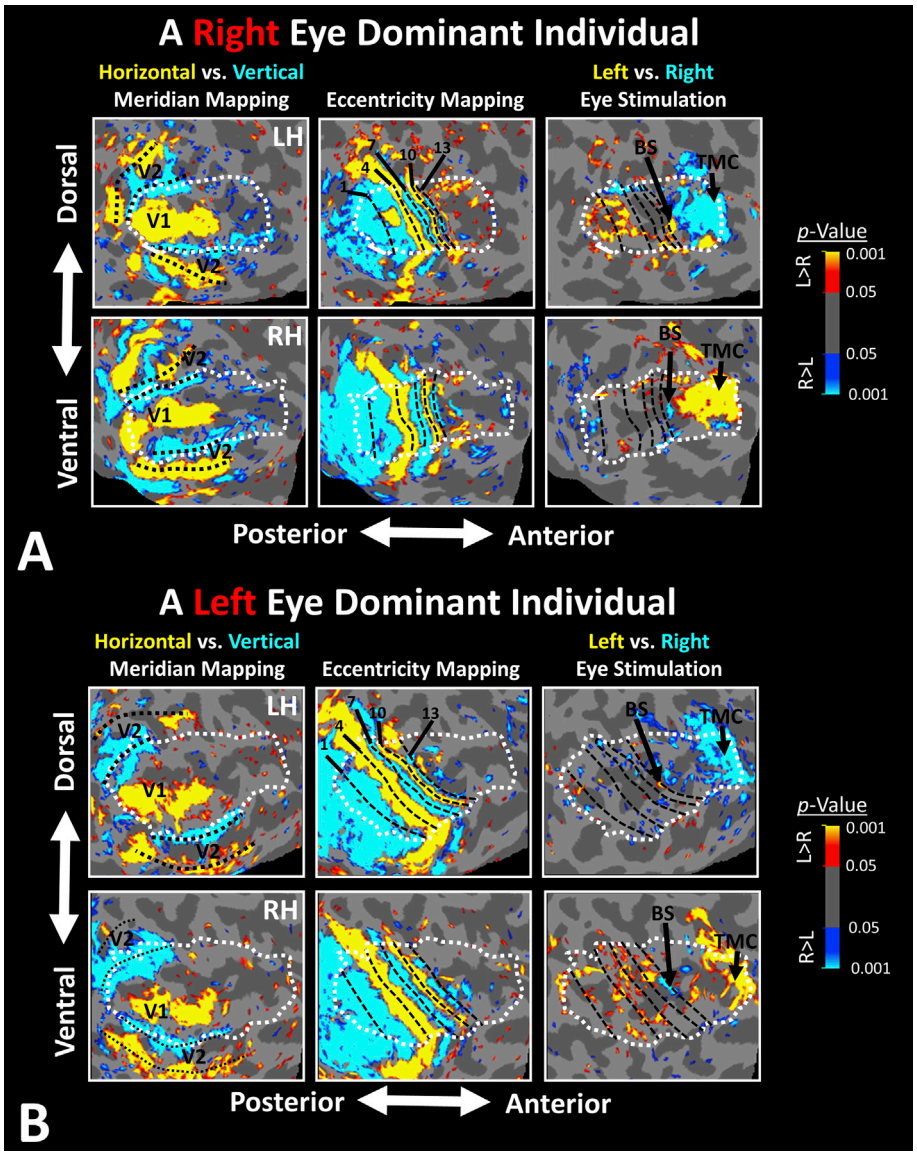

Fig. 3. Activity maps evoked by contrasting the response to stimulation of left vs. right eyes in two individual subjects. Panels **A** and **B** demonstrate the activity maps in a right-eye- and a left-eye-dominant individual, respectively. In each panel, the top and bottom rows show the activity maps collected within the left and right cortical hemispheres, respectively. For each subject, visuotopic representation of horizontal and vertical meridians were localized using independent sets of stimuli (see Methods) and overlaid in the reconstructed cortical surfaces shown in the **left** columns (black dotted lines). In the central visual field representations, these maps overlap with V1 borders estimated from the geometry of the folding pattern (white dotted lines (Hinds et al., 2008);). Representations of different eccentricities are demonstrated in the **middle** column (black dashed lines). Due to the known cortical magnification factor (Daniel and Whitteridge, 1961; Van Essen et al., 1984; Engel et al., 1997; Slotnick et al., 2001; Polimeni et al., 2006; Wandell et al., 2007), the extent of the cortex representing the ring patterns is expected to get smaller with increasing eccentricity, and therefore at this spatial resolution we could not resolve the cortical representation of eccentricities beyond 16°. The **right** column shows the location of TMC and blind spot representations, indicated by black arrows, relative to the borders of V1, defined both from anatomical estimates (white dotted lines) and from functional data derived from eccentricity mapping data (black dashed lines).

signal change for each vertex of the cortical surface reconstruction within V1, evoked by contrasting the response to right-vs. left-eye stimulation, and quantified this measure of activation amplitude independently for one half of the runs acquired in one experimental session, i.e., within all odd-numbered runs and also within all even-numbered runs. We then quantified the reproducibility of these contrast amplitudes by computing the Pearson test of correlation between responses evoked across odd-numbered and even-numbered runs in each subject and found a significant ($r > 0.57, p < 0.01$) correlation (Fig. 4A), indicating a high level of reproducibility across runs. Second, for right-eye-dominant subjects ($n = 4$), we measured the BOLD responses collected across two separate experimental sessions with more than a day gap between them (see Methods). Here again, quantification of the Pearson test of correlation showed a significant ($r > 0.65, p < 0.01$) reproducibility of the measured activations between activity evoked across the two scan sessions (Fig. 4B). Since it could be argued that the potential correlation within/between sessions is complicated by non-independence of activity in adjacent vertices due, for example, to spatial smoothness in the data, we also applied a stricter test based on non-parametric resampling statistics: for each within- or between-session correlation test, instead of testing all V1 vertices, we randomly selected 10% of the vertices within V1 and measured the level of correlation between their activities either across odd-numbered and even-numbered runs (in all subjects) for the within-session test or across the two sessions (of the right-eye-dominant subjects) for the across-session test. These correlation coefficients were compared relative to the chance level, defined as the level of correlation after randomly misaligning (i.e., spatially 'shuffling') the V1 vertices. We repeated this test 10,000 times for each subject. In all subjects, we found the probability of finding a correlation coefficient that was less than the correlation coefficient of randomly misaligned vertices (i.e., the null hypothesis) was less than 0.01. These results support the reliability/reproducibility of these activity maps both within and between scan sessions.

We then tested the consistency of the TMC representation localization between individual subjects. To reduce the impact of 'structural' differences across subjects, we re-mapped each subject's activation pattern from their native space into the *fsaverage* surface-based atlas space as a common template of the cerebral cortical surface (Fischl, 2012). Group-averaged ($n = 8$) activity maps were generated through a random-effects model (see Methods) and the resultant maps were corrected for multiple comparisons. As demonstrated in Fig. 5A, in both hemispheres a preference for contralateral eye stimulation was apparent within the most anterior portion of V1. Consistent with the maps observed in individual subjects (Fig. 3), we only found a comparably

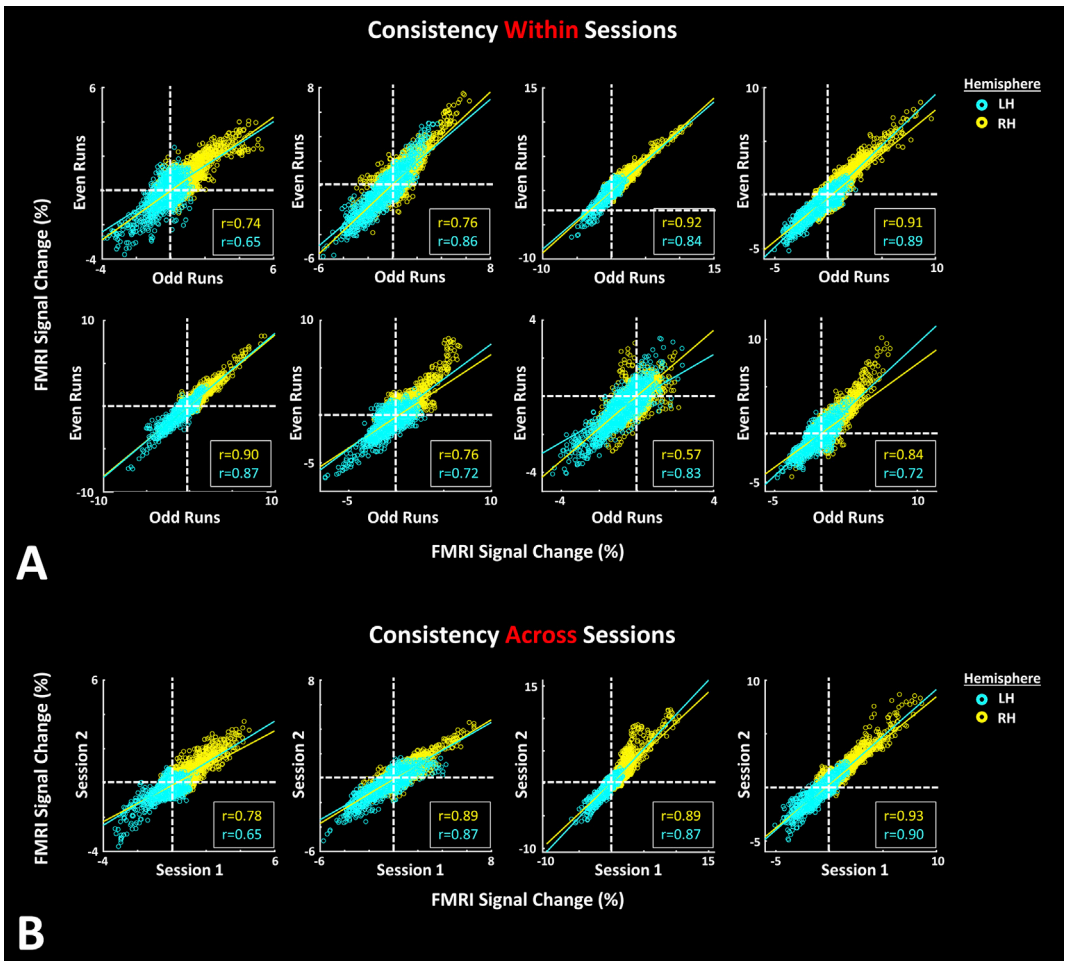

Fig. 4. Quantification of the consistency of activation within and across scan sessions. Panel **A** shows fMRI activity in response to 'left – right' contrast, with each point in the scatter plot representing activation from a single V1 vertex from the left (cyan) and right (yellow) cortical hemispheres, across odd-numbered and even-numbered runs. Each graph shows data from one individual subject. In all individuals ($n = 8$) we found a significant correlation between activity evoked across odd-numbered and even-numbered runs ($p < 0.01$). Panel **B** the same analysis was performed for activation consistency across rather than within sessions, based on the results from right-eye-dominant individuals ($n = 4$) who were scanned twice in two separate days. Again we found a significant correlation between the level of activity evoked within V1 vertices across the two scan session ($p < 0.01$).

limited extension of the TMC representation into the adjacent visual areas (i.e., V2) (see Discussion). These results demonstrate a consistency in the location of the putative TMC representation across subjects.

We further tested the consistency of the blind spot representation localization in contralateral hemispheres relative to the dominant eye. Fig. 5B shows group-averaged activity maps ($n = 4$), evoked by contrasting the response to left-eye vs. right-eye stimulation, within the left and right hemispheres of right- and left-eye-dominant individuals, respectively. Interestingly, despite the small size of the blind spot representation, we were still able to detect this region bilaterally in the expected visuotopic location based on the individual subject maps (Fig. 5C). For this consistency test, activity maps from individual subjects were transferred again from native space into *fsaverage* space to reduce the impact of structural differences across subjects on the location of the blind spot representation. This result demonstrates the consistency of the blind spot representation in our small group of subjects, when between-subject structural differences were addressed properly through the use of surface-based spatial normalization.

Finally, we checked the consistency of the TMC representation localization between activity maps in group-average vs. individual-subject levels. In this test, we defined a region of interest (ROI) based on the TMC representation derived from the group-averaged activity maps and then measured the activity levels within this ROI projected back into each individual subject's native space (i.e., after transforming the ROI from *fsaverage* space into each subject's surface reconstruction in native space). Fig. 6 shows the measured activity, evoked by contrasting the response to stimulation of the left vs. right eye, for each individual subject. Application of a two-factor repeated-measures ANOVA—stimulated-eye (ipsilateral vs. contralateral) and hemisphere (left vs. right)—to the measured activity showed a significantly stronger response to stimulation of contra-compared to ipsilateral eye stimulation (F (1, 6) = 68.85, $p < 10^{-3}$) and no significant effect of hemisphere (F (1, 6) = 1.96, $p = 0.21$) and/or a significant interaction between the two effects (F (1, 6) = 2.64, $p = 0.16$). This result support the consistency of the localization of the TMC representation across subjects, despite its relatively small size (Horton et al., 1990; Adams et al., 2007).

4. Discussion

In this study, we have presented *in vivo* functional evidence for the cortical visuotopic representation of the TMC, a portion of the visual field seen monocularly only by the contralateral eye. According to our findings, the TMC representation was localized in multiple individual subjects ($n = 8$) and in group-averaged activation maps in the most anterior portion of area V1 centered on the calcarine sulcus, consistent with previous studies in which the TMC representation was localized histologically (Horton et al., 1990; Adams et al., 2007). This was enabled by our use of MRI-compatible goggles that are capable of both delivering

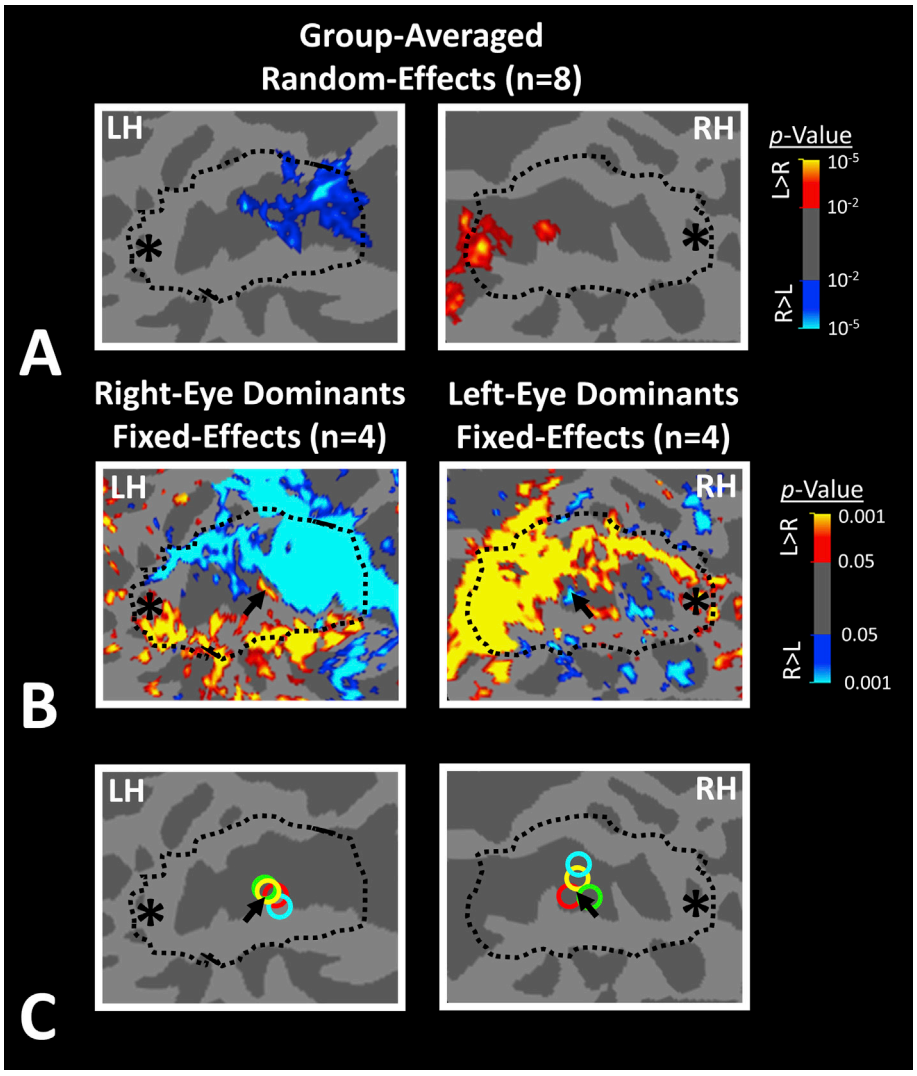

Fig. 5. Group-averaged activity maps generated by contrasting the response to stimulation of left vs. right eyes, overlaid on a common surface-based template. Panel **A** shows the activity maps generated based on a random-effects model ($n = 8$) after correction for multiple-comparisons. In both hemispheres, the TMC representations are localized significantly ($p < 0.05$) and at the opposite end of V1 relative to the central-field representation (indicated by asterisks), as expected from histological studies (Adams et al., 2007). Panel **B** shows the activity maps, generated based on a fixed-effects model ($n = 4$), within the hemispheres opposite to the dominant eye (i.e., right and left hemispheres in left- and right-eye-dominant individuals respectively). Location of the blind spot representation is indicated by a black arrow. In this panel, group-level maps were not corrected for multiple comparisons to avoid the elimination of the blind spot patch due to its small size and the small number of subjects. Panel **C** shows the location of the blind spot representation in individual subjects, each indicated with a different color marker; for reference, the location of the blind spot representation derived from the group-averaged activity maps is indicated by the black arrow as shown in Panel **B**. The consistency in the location of the blind spot representation is apparent across individuals when all activity maps are overlaid on a common surface-based brain template to account for structural variability of the cortex across subjects. In all maps, the estimated V1 border and the central-field representations are indicated by black dotted lines and asterisks, respectively.

monocular stimuli to each eye independently and stimulating the most far-peripheral portion of the visual field which is typically inaccessible when using conventional stimulus delivery approaches.

4.1. Anomalies in the spatial pattern of ocular dominance columns

Ocular dominance columns are considered a key feature of the functional architecture of the primary visual cortical area, V1. Columns with opposite ocular preference are typically organized within parallel 'stripes' distributed across V1. Histological studies have shown two major anomalies in the distribution of ocular dominance column stripes due to the blind spot and TMC representations. Specifically, in each hemisphere, the ipsilateral blind spot representation is apparent mainly due to the absence of ocular dominance columns that respond to stimulation of contralateral eye, resulting in a region consisting only of columns with an ipsilateral eye dominance. The portion of V1 that represents TMC is populated by those ocular dominance columns that respond to the stimulation of the contralateral eye. In this regard, both the blind spot and the TMC representations can be viewed as aggregations of several ocular dominance columns that interrupt the overall stripe pattern laid out along the cortical surface within V1.

Here we demonstrated consistency in the localization of these two anomalies in the distribution of ocular dominance columns using an analysis that accounted for inter-subject variability in the geometric properties (e.g., folding pattern and size) of V1. In all tested subjects, the TMC representation was detected bilaterally in the most anterior portion of V1, while the blind spot representation was localized adjacent to the representation of the ring stimulus presented at 15° visual field eccentricity, and along the horizontal meridian representation, in the contralateral hemisphere relative to the dominant eye. These findings suggest that these anomalies can be used as landmarks in studies of V1 during wide-field stimulus presentation.

4.2. Neuroimaging studies of ocular dominance columns

Neuroimaging studies of ocular dominance columns can be divided into two groups. The first group of studies aimed at revealing the ocular dominance columns, organized in stripe-like patterns within V1 (Menon et al., 1997; Cheng et al., 2001; Yacoub et al., 2007; Nasr et al., 2016). These studies typically took advantage of small voxels (≤1 mm in-plane resolution) achievable with ultra-high field MRI scanners (4T and 7T) (Yacoub et al., 2008). The second group aimed at revealing the blind spot representation (Tootell et al., 1998; Awater et al., 2005) which is an anomaly in the ocular dominance column stripe pattern. With regard to the larger size of the blind spot representation (>5 mm) compared to the size of individual ocular dominance column stripes (~1.5 mm center-to-center), this second group of studies used larger voxel size (>2 mm) to increase the field view necessary to sufficiently cover V1 and to improve the signal-to-noise ratio.

In the present study, similar to the second group of studies mentioned

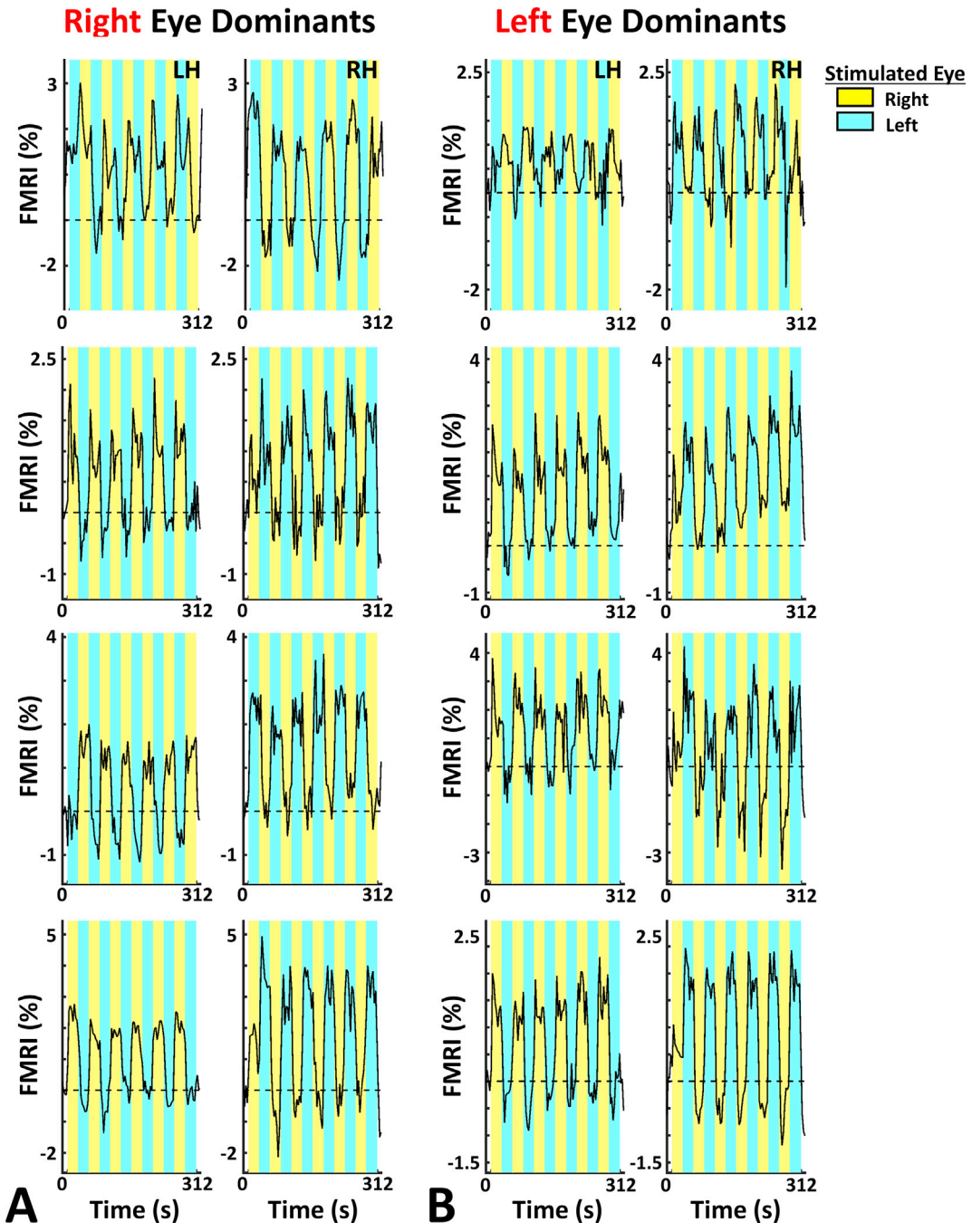

Fig. 6. Temporal pattern of activity evoked within the TMC representation ROI, defined based on group-averaged activity maps, in response to left-eye vs. right-eye stimulation in all eight individual subjects. Panels **A** and **B** show BOLD time courses, in units of percent signal change, in response to visual stimulation evoked within the TMC representation ROI in the right- and the left-eye dominant individuals, respectively. In both groups of individuals, stimulation of the contralateral eye triggers an activity increase in the TMC representation ROI. In all panels, baseline activation level during the period prior to stimulation is indicated by dashed lines.

above, we focused on revealing the anomalies in the spatial pattern of ocular dominance column organization. By taking advantage of MRI-compatible goggles, we increased the extent of the stimulated visual field beyond what was achieved in these previous studies (typically $< 40°$(Tootell et al., 1998; Awater et al., 2005)). This technical innovation enabled us to reveal the functional evidence for the TMC representation that is consistent with its known spatial layout based on histological data, and to clarify its location relative to the borders of V1. However, due to the relatively larger voxel size (1.2 mm isotropic) and lower fMRI detection sensitivity at 3T, compared to our previous studies conducted at 7T (e.g. see (Nasr et al., 2016)), the stripe-like pattern of ocular dominance columns was not apparent in our maps (Fig. 3). Because of the size and configuration of the RF receive coil array housings available at 3T and 7T, there was additional space available in our 3T scanner to comfortably accommodate the goggles. However, this goggle design is compatible with 7T MRI scanning as well (and has passed safety tests at 7T).

4.3. The TMC representation in V1 vs. V2

Our results, especially in group-averaged activity maps, suggest either a comparably smaller TMC representation in the second visual area, V2. At the first glance, this phenomenon may appear unexpected due to typical repetition of visual field representations across visual areas

(Sereno et al., 1995; Engel et al., 1997). However, it is widely known that neurons within higher tiers of the visual cortex have (on average) larger receptive fields compared to neurons within the lower tiers (Smith et al., 2001; Dumoulin and Wandell, 2008), and diminished ocular dominance (Horton et al., 1990; Adams et al., 2007). Considering this phenomenon, smaller TMC representation in V2 (compared to V1) is perhaps partly due to a decrease in the number of V2 neurons that receive input 'solely' from V1 neurons within the TMC representation. Although this finding does not rule out the existence of an ocular dominance response in V2 in a smaller scale compared to V1, it appears consistent with histological studies showing no apparent cluster of neurons with detectable eye-dominant responses within the anterior portion of V2 (Adams et al., 2007).

This abrupt change in the representation of features of the visual field, between V1 and V2, is not limited to the TMC representation. Rather, histological and neuroimaging studies have shown that ocular dominance columns in general, and the blind spot representation in particular, are also not found beyond V1 (Tootell et al., 1998; Awater et al., 2005; Adams et al., 2007).

4.4. Previous neuroimaging studies of peripheral vision

As mentioned above, Toosy and colleagues showed a stronger response to contralateral (compared to ipsilateral) visual stimulation in anterior portions of visual cortex following monocular stimulation. However, the exact location of this response relative to the borders of V1, the agreement of the spatial pattern of this representation with the known pattern from anatomical studies (Adams et al., 2007), and also its consistency across individuals remained mostly unknown (Toosy et al., 2001). In addition to this prior study, multiple other previous fMRI studies have also succeeded in stimulating the peripheral visual field. For instance, Tootell et al. (1998) instructed their subjects to gaze at a peripherally (rather than centrally) presented fixation target to extend the lateral extension of the stimulated visual field to almost 20° (see also (Nasr et al., 2011)). Although this method enabled them to successfully localize the blind spot representation in their subjects, it limited the stimulated visual field to only one hemifield (either left or right) at a time.

Other studies have achieved larger extents of the stimulated visual fields (up to ±60°) by reducing the distance between the screen and the subjects' eyes and using curved screens and/or contact lenses (Cheng et al., 1995; Pitzalis et al., 2006; Arnoldussen et al., 2011; Wu et al., 2012, 2013). Despite this improvement, these methods require a relatively short distance between the projector and subject which may necessitate specialized non-magnetic projector hardware. Notably, the stimulated visual field achieved by this approach is still not sufficient to drive activation within the TMC representation, which requires visual stimulation up to 100° eccentricity. Consequently, previous visuotopic mapping studies based on this approach (e.g., see (Wu et al., 2012)) usually failed to extend their mapping to the most anterior parts of the calcarine sulcus in which the far visual representation is expected (Hinds et al., 2008).

Another approach to enlarge the stimulated visual field relies on using MRI-compatible goggles. MRI-compatible liquid crystal displays (LCDs) and/or fiber optics have been used successfully in studies of virtual reality and 3D perception (e.g. (Cornelissen et al., 1997; Hoffman et al., 2003; Mraz et al., 2003; Henning et al., 2005; Huang and Sereno, 2008),). Although using these goggles can enlarge the stimulated visual field compared to the conventional methods of stimulus presentation, they cannot stimulate the visual field beyond 50° eccentricity (Stenbacka and Vanni, 2007). This is mainly due to the flat (rather than curved) screens implemented in these devices.

5. Conclusions

In this study we have used a custom stimulus delivery apparatus to stimulate the full visual field in each eye independently within the MRI scanner, and used this to map the visuotopic representations of both the blind spot and TMC regions of the visual field. These regions are challenging to image because (*i*) they are relatively small compared to the size of voxels that is used in conventional fMRI studies in humans, (*ii*) conventional visual stimulation is presented to both eyes simultaneously, and (*iii*) visual stimulation usually extends to about 10°–15° eccentricity. We reliably detected eye-dominant responses within V1 that were consistent with the expected location of both the blind spot and TMC representations.

Author contribution

Shahin Nasr: Conceptualization, Investigation, Validation, Formal analysis, Writing - Original Draft, Visualization.

Cristen LaPierre: Resources, Software.

Christopher E. Vaughn: Resources, Software.

Thomas Witzel: Resources.

Jason P. Stockmann: Resources, Investigation.

Jonathan R. Polimeni: Conceptualization, Writing - Review & Editing, Supervision, Project administration, Funding acquisition.

Declaration of competing interest

The authors declare no conflict of interest.

Acknowledgments

We thank Mr. Ned Ohringer for his help with volunteer recruitment and data collection. This work was supported in part by the NIH NIBIB (grants P41-EB015896, and R01-EB019437), NEI (grant R01-EY026881), by the *BRAIN Initiative* (NIH NIMH grant R01-MH111419 and R01-MH111438), and by the MGH/HST Athinoula A. Martinos Center for Biomedical Imaging; and was made possible by resources provided by the NIH Shared Instrumentation Grant S10-RR019371.

References

Adams, D.L., Sincich, L.C., Horton, J.C., 2007. Complete pattern of ocular dominance columns in human primary visual cortex. J. Neurosci. 27, 10391–10403.

Arnoldussen, D.M., Goossens, J., van den Berg, A.V., 2011. Adjacent visual representations of self-motion in different reference frames. Proc. Natl. Acad. Sci. 108, 11668–11673.

Awater, H., Kerlin, J.R., Evans, K.K., Tong, F., 2005. Cortical representation of space around the blind spot. J. Neurophysiol. 94, 3314–3324.

Barton, K.R., Valtchanov, D., Ellard, C., 2014. Seeing beyond your visual field: the influence of spatial topology and visual field on navigation performance. Environ. Behav. 46, 507–529.

Cheng, K., Fujita, H., Kanno, I., Miura, S., Tanaka, K., 1995. Human cortical regions activated by wide-field visual motion: an H2 (15) O PET study. J. Neurophysiol. 74, 413–427.

Cheng, K., Waggoner, R.A., Tanaka, K., 2001. Human ocular dominance columns as revealed by high-field functional magnetic resonance imaging. Neuron 32, 359–374.

Cornelissen, F.W., Pelli, D.G., Farell, B., Huckins, S.C., Szeverenyi, N.M., 1997. A binocular fiberscope for presenting visual stimuli during fMRI. Spat. Vis. 11, 75–82.

Dale, A.M., Fischl, B., Sereno, M.I., 1999. Cortical surface-based analysis. I. Segmentation and surface reconstruction. Neuroimage 9, 179–194.

Daniel, P., Whitteridge, D., 1961. The representation of the visual field on the cerebral cortex in monkeys. J. Physiol. 159, 203–221.

Dumoulin, S.O., Wandell, B.A., 2008. Population receptive field estimates in human visual cortex. Neuroimage 39, 647–660.

Duncan, R.O., Boynton, G.M., 2003. Cortical magnification within human primary visual cortex correlates with acuity thresholds. Neuron 38, 659–671.

Engel, S.A., Glover, G.H., Wandell, B.A., 1997. Retinotopic organization in human visual cortex and the spatial precision of functional MRI. Cerebr. Cortex 7, 181–192.

Fischl, B., 2012. FreeSurfer. Neuroimage 62, 774–781.

Fischl, B., Salat, D.H., Busa, E., Albert, M., Dieterich, M., Haselgrove, C., van der Kouwe, A., Killiany, R., Kennedy, D., Klaveness, S., Montillo, A., Makris, N., Rosen, B., Dale, A.M., 2002. Whole brain segmentation: automated labeling of neuroanatomical structures in the human brain. Neuron 33, 341–355.

Fischl, B., Sereno, M.I., Dale, A.M., 1999. Cortical surface-based analysis. II: inflation, flattening, and a surface-based coordinate system. Neuroimage 9, 195–207.

Friston, K.J., Holmes, A.P., Price, C.J., Buchel, C., Worsley, K.J., 1999. Multisubject fMRI studies and conjunction analyses. Neuroimage 10, 385–396.

Gattass, R., Sousa, A.P., Rosa, M.G., 1987. Visual topography of V1 in the Cebus monkey. J. Comp. Neurol. 259, 529–548.
Greco, V., Frijia, F., Mikellidou, K., Montanaro, D., Farini, A., D'Uva, M., Poggi, P., Pucci, M., Sordini, A., Morrone, M.C., 2016. A low-cost and versatile system for projecting wide-field visual stimuli within fMRI scanners. Behav. Res. Methods 48, 614–620.
Greve, D.N., Fischl, B., 2009. Accurate and robust brain image alignment using boundary-based registration. Neuroimage 48, 63–72.
Henderson, J.M., Anes, M.D., 1994. Roles of object-file review and type priming in visual identification within and across eye fixations. J. Exp. Psychol. Hum. Percept. Perform. 20, 826.
Henning, S., Merboldt, K.D., Frahm, J., 2005. Simultaneous recordings of visual evoked potentials and BOLD MRI activations in response to visual motion processing. NMR Biomed.: An International Journal Devoted to the Development and Application of Magnetic Resonance In vivo 18, 543–552.
Hinds, O.P., Rajendran, N., Polimeni, J.R., Augustinack, J.C., Wiggins, G., Wald, L.L., Diana Rosas, H., Potthast, A., Schwartz, E.L., Fischl, B., 2008. Accurate prediction of V1 location from cortical folds in a surface coordinate system. Neuroimage 39, 1585–1599.
Hoffman, H.G., Richards, T.L., Magula, J., Seibel, E.J., Hayes, C., Mathis, M., Sharar, S.R., Maravilla, K., 2003. A magnet-friendly virtual reality fiberoptic image delivery system. Cyberpsychol. Behav. 6, 645–648.
Horton, J.C., Dagi, L.R., McCrane, E.P., de Monasterio, F.M., 1990. Arrangement of ocular dominance columns in human visual cortex. Arch. Ophthalmol. 108, 1025–1031.
Horton, J.C., Hocking, D.R., 1996. Intrinsic variability of ocular dominance column periodicity in normal macaque monkeys. J. Neurosci. 16, 7228–7239.
Huang, R.-S., Sereno, M.I., 2008. Visual stimulus presentation using fiber optics in the MRI scanner. J. Neurosci. Methods 169, 76–83.
Li, J., Lam, C.S., Yu, M., Hess, R.F., Chan, L.Y., Maehara, G., Woo, G.C., Thompson, B., 2010. Quantifying sensory eye dominance in the normal visual system: a new technique and insights into variation across traditional tests. Investig. Ophthalmol. Vis. Sci. 51, 6875–6881.
Menon, R.S., Ogawa, S., Strupp, J.P., Ugurbil, K., 1997. Ocular dominance in human V1 demonstrated by functional magnetic resonance imaging. J. Neurophysiol. 77, 2780–2787.
Mraz, R., Hong, J., Quintin, G., Staines, W.R., McIlroy, W.E., Zakzanis, K.K., Graham, S.J., 2003. A platform for combining virtual reality experiments with functional magnetic resonance imaging. Cyberpsychol. Behav. 6, 359–368.
Nasr, S., Liu, N., Devaney, K.J., Yue, X., Rajimehr, R., Ungerleider, L.G., Tootell, R.B., 2011. Scene-selective cortical regions in human and nonhuman primates. J. Neurosci. 31, 13771–13785.
Nasr, S., Polimeni, J.R., Tootell, R.B., 2016. Interdigitated color- and disparity-selective columns within human visual cortical areas V2 and V3. J. Neurosci. 36, 1841–1857.
Pitzalis, S., Galletti, C., Huang, R.-S., Patria, F., Committeri, G., Galati, G., Fattori, P., Sereno, M.I., 2006. Wide-field retinotopy defines human cortical visual area V6. J. Neurosci. 26, 7962–7973.
Polimeni, J.R., Balasubramanian, M., Schwartz, E.L., 2006. Multi-area visuotopic map complexes in macaque striate and extra-striate cortex. Vis. Res. 46, 3336–3359.
Pollatsek, A., Rayner, K., Henderson, J.M., 1990. Role of spatial location in integration of pictorial information across saccades. J. Exp. Psychol. Hum. Percept. Perform. 16, 199.
Rice, M.L., Leske, D.A., Smestad, C.E., Holmes, J.M., 2008. Results of ocular dominance testing depend on assessment method. J. Am. Assoc. Pediatr. Ophthalmol. Strabismus 12, 365–369.
Rombouts, S.A., Barkhof, F., Sprenger, M., Valk, J., Scheltens, P., 1996. The functional basis of ocular dominance: functional MRI (fMRI) findings. Neurosci. Lett. 221, 1–4.
Rosenholtz, R., Huang, J., Raj, A., Balas, B.J., Ilie, L., 2012. A summary statistic representation in peripheral vision explains visual search. J. Vis. 12, 14-14.
Sereno, M.I., Dale, A.M., Reppas, J.B., Kwong, K.K., Belliveau, J.W., Brady, T.J., Rosen, B.R., Tootell, R.B., 1995. Borders of multiple visual areas in humans revealed by functional magnetic resonance imaging. Science 268, 889–893.
Slotnick, S.D., Klein, S.A., Carney, T., Sutter, E.E., 2001. Electrophysiological estimate of human cortical magnification. Clin. Neurophysiol. 112, 1349–1356.
Smith, A.T., Singh, K.D., Williams, A., Greenlee, M., 2001. Estimating receptive field size from fMRI data in human striate and extrastriate visual cortex. Cerebr. Cortex 11, 1182–1190.
Stenbacka, L., Vanni, S., 2007. fMRI of peripheral visual field representation. Clin. Neurophysiol. 118, 1303–1314.
Tong, F., Engel, S.A., 2001. Interocular rivalry revealed in the human cortical blind-spot representation. Nature 411, 195.
Toosy, A., Werring, D., Plant, G., Bullmore, E., Miller, D., Thompson, A., 2001. Asymmetrical activation of human visual cortex demonstrated by functional MRI with monocular stimulation. Neuroimage 14, 632–641.
Tootell, R.B., Hadjikhani, N.K., Vanduffel, W., Liu, A.K., Mendola, J.D., Sereno, M.I., Dale, A.M., 1998. Functional analysis of primary visual cortex (V1) in humans. Proc. Natl. Acad. Sci. 95, 811–817.
Tootell, R.B., Taylor, J.B., 1995. Anatomical evidence for MT and additional cortical visual areas in humans. Cerebr. Cortex 5, 39–55.
Van Essen, D.C., Newsome, W.T., Maunsell, J.H., 1984. The visual field representation in striate cortex of the macaque monkey: asymmetries, anisotropies, and individual variability. Vis. Res. 24, 429–448.
Wandell, B.A., Dumoulin, S.O., Brewer, A.A., 2007. Visual field maps in human cortex. Neuron 56, 366–383.
Wilson, H.R., 1990. The perception of form: retina to striate cortex. Visual perception: The neurophysiological foundations 231–272.
Wu, J., Wang, B., Yang, J., Hikino, Y., Takahashi, S., Yan, T., Ohno, S., Kanazawa, S., 2013. Development of a method to present wide-view visual stimuli in MRI for peripheral visual studies. J. Neurosci. Methods 214, 126–136.
Wu, J., Yan, T., Zhang, Z., Jin, F., Guo, Q., 2012. Retinotopic mapping of the peripheral visual field to human visual cortex by functional magnetic resonance imaging. Hum. Brain Mapp. 33, 1727–1740.
Yacoub, E., Harel, N., Ugurbil, K., 2008. High-field fMRI unveils orientation columns in humans. Proc. Natl. Acad. Sci. U. S. A. 105, 10607–10612.
Yacoub, E., Shmuel, A., Logothetis, N., Ugurbil, K., 2007. Robust detection of ocular dominance columns in humans using Hahn Spin Echo BOLD functional MRI at 7 Tesla. Neuroimage 37, 1161–1177.
Young, T., 1801. II. The Bakerian Lecture. On the Mechanism of the Eye. Philosophical Transactions of the Royal Society of London, pp. 23–88.